Earth and Planetary Science Letters 494 (2018) 69–82

Contents lists available at ScienceDirect

Earth and Planetary Science Letters

www.elsevier.com/locate/epsl

Particle size distributions in chondritic meteorites: Evidence for pre-planetesimal histories

J.I. Simon [a,*], J.N. Cuzzi [b], K.A. McCain [c,1,2], M.J. Cato [d,1,3], P.A. Christoffersen [e,1,4], K.R. Fisher [f,1,5], P. Srinivasan [g,1,3], A.W. Tait [h,1,6], D.M. Olson [i], J.D. Scargle [b]

[a] Center for Isotope Cosmochemistry and Geochronology, ARES, EISD-XI3, NASA Johnson Space Center, Houston, TX 77058, USA
[b] NASA Ames Research Center, Moffett Field, CA 94035, USA
[c] The University of Chicago, Chicago, IL 60637, USA
[d] Western Carolina University, Cullowhee, NC, 28723, USA
[e] St. Lawrence University, Canton, NY, 13617, USA
[f] University of Cincinnati, Cincinnati, OH, 45219, USA
[g] Rutgers University, Piscataway, NJ, 08854, USA
[h] Monash University, Clayton, 3168, VIC, Australia
[i] BAERI, inc., Petaluma, CA 94952, USA

ARTICLE INFO

Article history:
Received 6 February 2018
Received in revised form 11 April 2018
Accepted 12 April 2018
Available online 17 May 2018
Editor: F. Moynier

Keywords:
chondritic meteorites
chondrules
CAIs
planetesimals
protoplanetary disks
asteroids

ABSTRACT

Magnesium-rich silicate chondrules and calcium-, aluminum-rich refractory inclusions (CAIs) are fundamental components of primitive chondritic meteorites. It has been suggested that concentration of these early-formed particles by nebular sorting processes may lead to accretion of planetesimals, the planetary bodies that represent the building blocks of the terrestrial planets. In this case, the size distributions of the particles may constrain the accretion process. Here we present new particle size distribution data for Northwest Africa 5717, a primitive ordinary chondrite (ungrouped 3.05) and the well-known carbonaceous chondrite Allende (CV3). Instead of the relatively narrow size distributions obtained in previous studies (Ebel et al., 2016; Friedrich et al., 2015; Paque and Cuzzi, 1997, and references therein), we observed broad size distributions for all particle types in both meteorites. Detailed microscopic image analysis of Allende shows differences in the size distributions of chondrule subtypes, but collectively these subpopulations comprise a composite "chondrule" size distribution that is similar to the broad size distribution found for CAIs. Also, we find accretionary 'dust' rims on only a subset (~15–20%) of the chondrules contained in Allende, which indicates that subpopulations of chondrules experienced distinct histories prior to planetary accretion. For the rimmed subset, we find positive correlation between rim thickness and chondrule size. The remarkable similarity between the size distributions of various subgroups of particles, both with and without fine grained rims, implies a common size sorting process. Chondrite classification schemes, astrophysical disk models that predict a narrow chondrule size population and/or a common localized formation event, and conventional particle analysis methods must all be critically reevaluated. We support the idea that distinct "lithologies" in NWA 5717 are nebular aggregates of chondrules. If ≥cm-sized aggregates of chondrules can form it will have implications for planet formation and suggests the sticking stage is where the preferential size physics is operating.

1. Introduction

Largely spherical, magnesium-rich silicate chondrules constitute 30–80% of primitive meteorites and have been reported to be narrowly size-sorted (Ebel et al., 2016, and references therein) as compared to more irregular shaped, refractory CAIs that make up

* Corresponding author.
E-mail address: justin.i.simon@NASA.gov (J.I. Simon).

[1] Former summer interns at JSC through Lunar and Planetary Institute or NASA Co-op Programs.

[2] Now at University of California, Los Angeles, Department of Earth, Planetary, and Space Sciences, Los Angeles, CA, 90095, USA.

[3] Now at University of New Mexico, Department of Earth and Planetary Sciences, Albuquerque, NM, 87131, USA.

[4] Now at Centre for Planetary Science and Exploration, Department of Earth Sciences, University of Western Ontario, London, Ontario, Canada, N6A 3K7.

[5] Now at ARES, NASA Johnson Space Center, Houston, TX, 77058, USA.

[6] Now at University of Stirling, Department of Biological and Environmental Sciences, Stirling, FK9 4LA, Scotland, UK.

https://doi.org/10.1016/j.epsl.2018.04.021

only 1–10% and thought to be less tightly sized-sorted (Hezel et al., 2008, references therein). The high abundances of chondrules in primitive meteorites suggest that chondrule formation and accumulation processes were fundamental to the earliest stages of the accretion of asteroids, which provide the parent bodies for these primitive meteorites. Since terrestrial planets formed from primitive asteroids or analogous planetesimals, understanding these early stages is important for understanding planetary accretion overall.

The mineralogical, chemical, and isotopic composition of chondritic components provide important constraints on their initial formation conditions (*e.g.*, Alexander et al., 2008; Davis et al., 2017; Gooding and Keil, 1981; Huang et al., 2012; Richter et al., 2002; Shahar and Young, 2007; Simon et al., 2017; Yu and Hewin, 1998). However, the characteristic distributions of particle sizes in primitive meteorites likely reflect a combination of how the various subgroups of particles initially formed (*e.g.*, Charnoz et al., 2015), at different times and in different locations in the solar nebula, and how they were preserved and/or were concentrated (*i.e.*, sorted) between formation and parent body assembly.

There are a number of hypotheses for the formation of chondrules. Most postulate that they originated from melting early-formed dust by either localized or nebula scale energetic events in the gas-rich stage of the protoplanetary disk (Boss, 1996; Connolly and Love, 1998; Grossman et al., 1989; Jones et al., 2000), such as magnetic flares (Levy and Araki, 1989), current sheets (Joung et al., 2004), lightning (Desch and Cuzzi, 2000; Johansen and Okuzumi, 2018) or nebular shock waves (Desch and Connolly, 2002; Morris and Desch, 2010; Wood, 1996). Alternative formation models include "melt splash" due to impacts on or between primitive planetary bodies (Johnson et al., 2015; Asphaug et al., 2011), or in planetesimal bow shocks (*e.g.*, Morris et al., 2012).

The more refractory mineralogy of CAIs implies that they formed from precursor materials that condensed out of nebula gas at a high temperature (Grossman et al., 2002), perhaps closer to the protoSun, or at an earlier, hotter nebula stage. There is evidence from radioisotopic age constraints that CAIs might be as much as ~2 Ma older than chondrules (*e.g.*, Connelly et al., 2012). Given the significant compositional differences (implying that they formed under very different conditions) and their likely age differences, the problem of how CAIs with high-temperature minerals ultimately end up mixed with chondrules and other lower temperature minerals remains a mystery (cf. Ciesla, 2010; Jacquet et al., 2011). These 'lucky' CAIs avoided being lost into the Sun or otherwise destroyed in the varied chaotic environments extant in the protosolar disk, including the thermal processes that produced chondrules. Partial overlap of the CAI and chondrule formation environments has been suggested, based on evidence that CAIs interacted with, and possibly some of their rims formed in a chondrule-like environment (Dyl et al., 2011; Simon et al., 2005; Simon and Young, 2011). Finally, the free-floating CAIs must also be 'selected' for accretion into the same planetesimal building block(s) as the chondrules.

In principle, size distributions of chondrules (*e.g.*, Ebel et al., 2016) and CAIs (*e.g.*, Hezel et al., 2008) in meteorites can be used to test astrophysical processes. However, with a few exceptions (*e.g.*, Teitler et al., 2010) the differences within and between these distinct particle groups, both of which are made up of diverse subgroups with different minerals and thermal histories, remain poorly quantified. McSween (1977) noted that CV chondrite chondrules ranged in diameter from ~550 μm to ~2000 μm. Grossman et al. (1989) reported a compiled mean diameter of ~1000 μm, but did not cite specific data sources. In abstract form, Paque and Cuzzi (1997) and May et al. (1999) reported mean chondrule diameter for CV chondrites from ~680 to 850 μm. Teitler et al. (2010) reevaluated the Paque and Cuzzi (1997) data, and along with additional disaggregated materials, reported mean diameters for Allende chondrules of 912 ± 644 μm ($n = 287$) and 917 ± 744 μm ($n = 126$). The available data for CAIs in Allende are more limited, but appear distinct from chondrules. McSween (1977) reported CAIs in terms of modal area fraction ranging from 2.5 to 9.4%. May et al. (1999) obtained a much smaller and narrower range between 0.65 and 1.89%. Hezel et al. (2008) found that CAIs make up 5.02 ± 0.80% ($n = 223$) of the modal area of three Allende thin sections, and based on these and the available literature data report that the modal area of CAIs in Allende is $2.98^{+0.3\%}_{-0.1\%}$. They also report a mean CAI diameter of ~100 μm with a pronounced peak at the smallest diameters (<100 μm). Their reported size distribution decreases monotonically to slightly larger sizes (~300 μm in diameter) and then shows a few, exceptionally large (1000's μm), outliers.

There have been a large number of size distribution studies of chondrules in ordinary chondrites. For a comprehensive view, see the excellent summary by Friedrich et al. (2015). There appears to be variability among the various chondrites (mean diameters differ from ~300 μm to ~1200 μm), but with a few exceptions, the data sets are relatively small and, like for the CV chondrites, the smallest and largest particles may have been undercounted, as discussed below.

Here we report a large-area, high-resolution study of the types and sizes of particles in the ordinary chondrite Northwest Africa 5717 ($n = 12{,}966$ particles measured in a photographic mosaic) and the well-studied carbonaceous chondrite Allende ($n = 2339/2555$ particles/particle cores measured in X-ray maps and $n = 6530$ particles in a photographic mosaic). With this extensive data set a number of important observations can be made: (1) The measured particle size distributions are significantly broader than previously reported. This spread in size is inconsistent with previous particle sorting models (Cuzzi et al., 2001) that predict narrow size distributions. In practical terms, the differences among the measured distributions highlight the fact that sampling bias is likely a systemic problem, a problem pointed out recently (*e.g.*, Ebel et al., 2016), and thus there is a need to reevaluate the current data and its use for defining "characteristic" particle sizes for classification purposes. (2) In Allende most (~85%) particles are unrimmed and in direct contact with meteorite host material (the matrix) whereas rims surround the other ~15%, often nearby, particles. This diverse behavior strongly argues for pre-accretional rim formation for some particles as they traversed distinct (cooler and/or dustier) nebular environments, *e.g.*, Metzler et al. (1992). (3) When present, fine-grained accretion rim types and thicknesses appear correlated to underlying particle size as recently reported for chondrules contained in the Murchison chondrite (Hanna and Ketcham, 2018). (4) Allende shows differences in the size distributions of chondrule subtypes, but collectively these subpopulations comprise a composite "chondrule" size distribution that is similar to the broad size distribution found for CAIs. And (5) NWA 5717 contains distinct lithologies that appear to be chondrule aggregates.

2. Methods

2.1. Sample materials

Northwest Africa 5717 is an ungrouped (subtype 3.05) ordinary chondrite dominated by chondrules, that contains two apparently distinct lithologies (Bigolski et al., 2016; Bunch et al., 2010). In the studied ~11 cm × 14 cm slab, the darker of these lithologies seems to host the second, much lighter lithology (Fig. 1). The nature of the boundary between the two is variable and at times uncertain, ranging from abrupt to gradational and not always following particle boundaries. The distinction between the lithologies, beyond the obvious color differences, has been supported by a

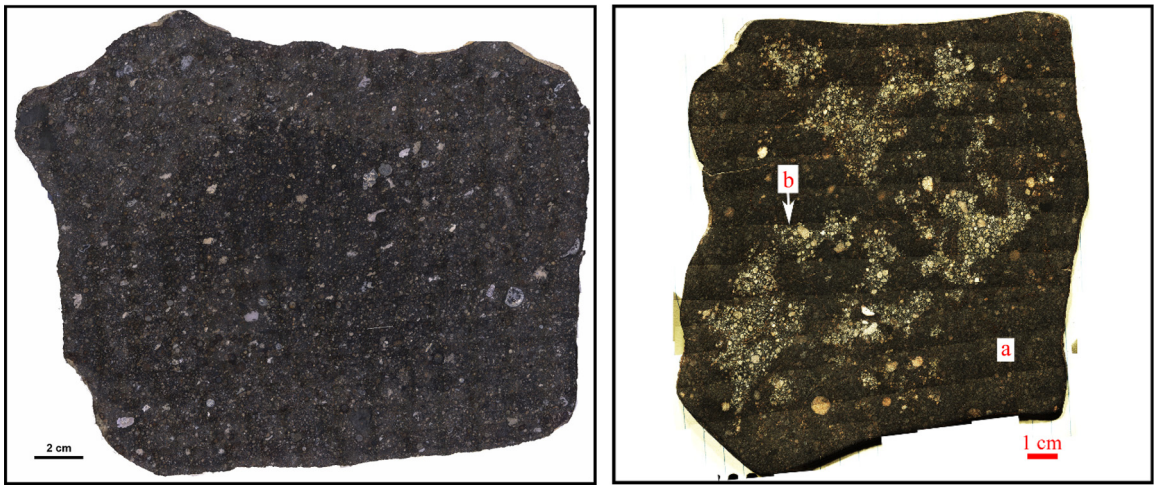

Fig. 1. Low-resolution optical photomosaic images of: (A) primitive CV3 Allende chondrite ~20 cm × 25 cm slab and (B) primitive (subtype 3.05) ungrouped chondrite NWA 5717 ~11 cm × 14 cm slab. In NWA 5717 the dark lithology is denoted by a and light by b.

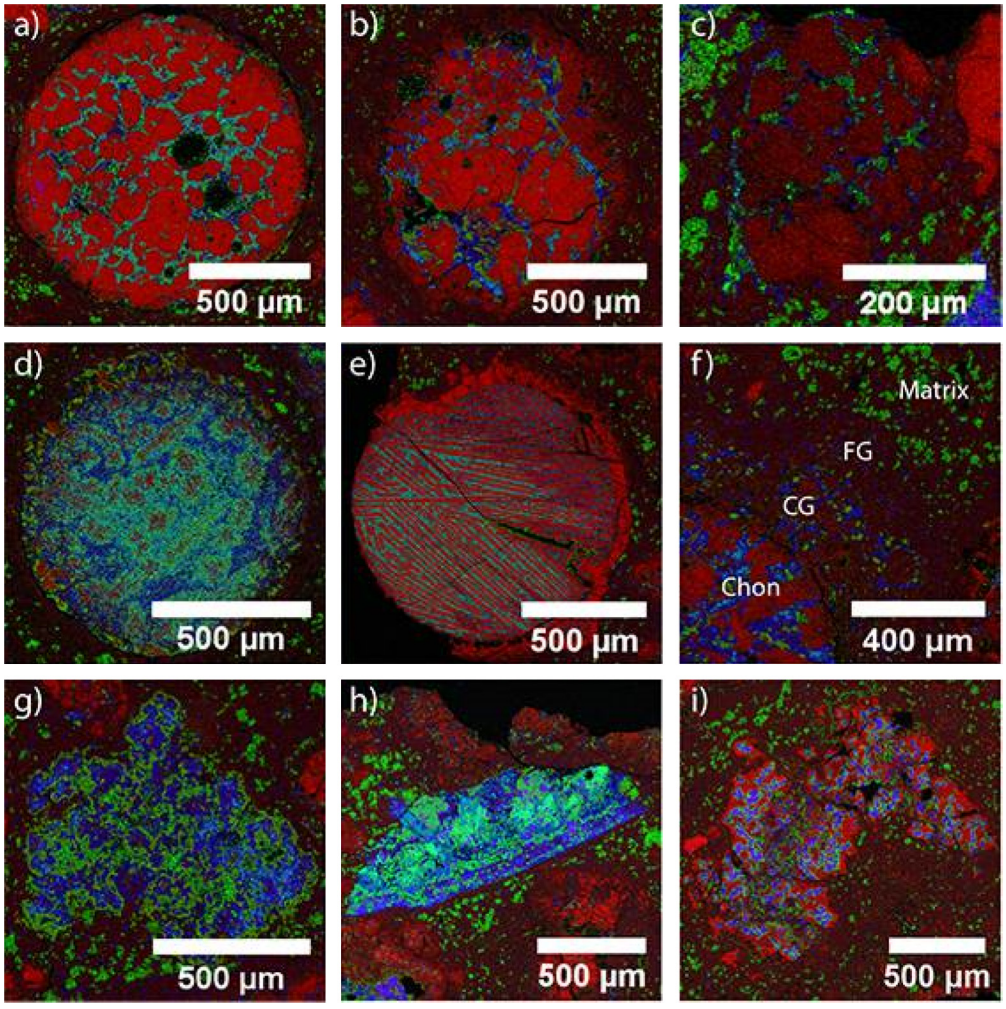

Fig. 2. Classification scheme (after Gooding and Keil, 1981) used to categorize particles in SEM X-ray compositional images, with Mg, Ca, and Al indicated by red, green, and blue, respectively. a) Porphyritic olivine chondrule (PO). b) Porphyritic olivine and pyroxene chondrule (POP). c) Porphyritic pyroxene chondrule (PP). d) Aluminum-rich chondrule. e) Barred olivine chondrule (BO). f) Coarse-grained (CG) and fine-grained chondrule rims. g) Type A CAI, h) Type B CAI. i) Amoeboid olivine aggregate (AOA). (For interpretation of the colors in the figure(s), the reader is referred to the web version of this article.)

discrepancy in oxygen isotopes and an incongruity in the magnesium contents of chondrule olivine (Bunch et al., 2010). Allende is a well-studied CV3 oxidized carbonaceous chondrite that contains a range of nebular components, including a diversity of chondrule types and refractory inclusions (Fig. 2). A large piece of the Allende meteorite was cut into ~cm thick slabs and one slab was gently broken into fragments that could be mounted in one inch epoxy rounds for scanning electron microscope (SEM) analysis. SEM im-

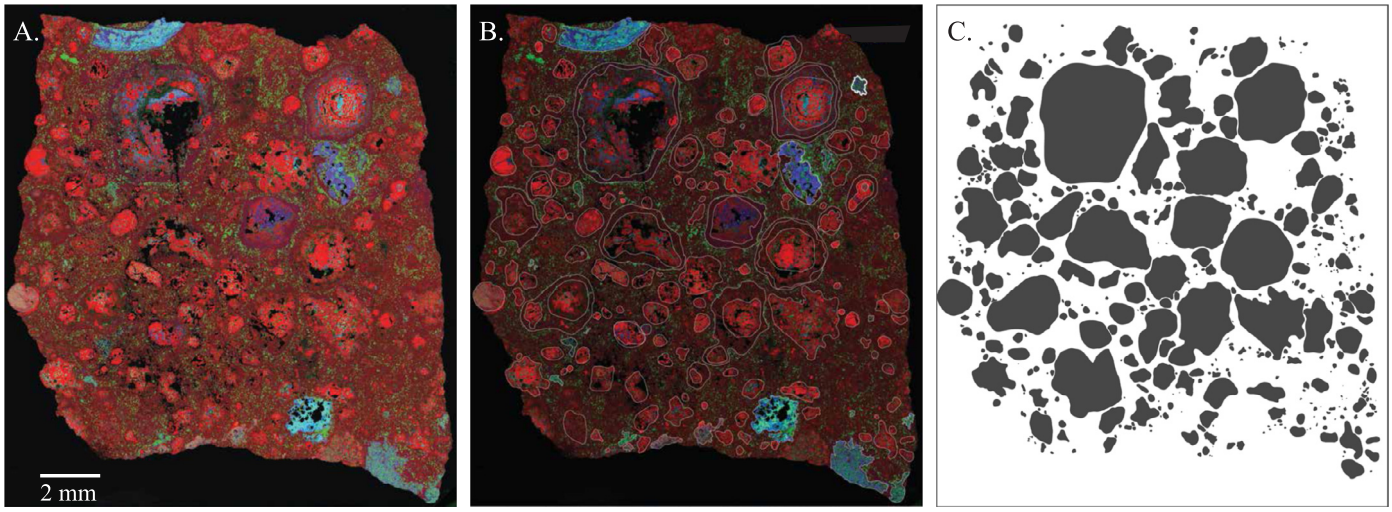

Fig. 3. (A) Representative example of X-ray compositional images for one section of the Allende chondritic meteorite, with color coding as in Fig. 2. (B) Digitized particles, including rim(s), and (C) ChonMax particles shown in binary image.

agery of several unassociated Allende slab fragments were also included in this study and help ensure wide sample representation.

Chemical phase maps, photomicrographic mosaics, and particle digitization

Energy-dispersive X-ray chemical maps were obtained by SEM analysis of six Allende fragment samples (0.86 cm^2, 1.52 cm^2, 1.82 cm^2, 1.86 cm^2, 1.91 cm^2, 2.11 cm^2 sized pieces) using the JEOL 7600 field emission SEM at NASA JSC. Images were acquired at 15 kV, 30 nA, with a 90 µm aperture. The images were taken at ~150× magnification with resolutions of 2.9–3.3 µm/pixel for a combined total area of 10.08 cm^2. Combination of characteristic X-ray emission from multiple elements was used to create chemical phase maps (maps are shown in supplemental Figs. S1–S6) in which all of the particles greater than ~50 µm in diameter were characterized. The images obtained for the Allende work were characterized by multiple investigators in a semi-blind manner detailed by Tait et al. (2016). No SEM data was acquired from NWA 5717.

Results obtained from X-ray image analyses (supplemental Table S1) were compared to results derived from a mosaic of photographic images obtained from a slab of Allende that is ~20 cm × 25 cm (Fig. 1, supplemental Fig. S7). A similar photomosaic was made for the NWA 5717 slab. Outlines of chondrules and CAIs were also obtained from the X-ray maps and used to create binary images of the sample particle subgroups (Fig. 3, Fig. S8). Based on the binary data, ImageJ was used to characterize the area and circularity of each individual particle and the modal area of each subgroup (Table S1). The size of each particle was calculated from the total pixels in each particle assuming a circular cross section (*i.e.*, diameter $= \sqrt{pixel\ area/\pi} \times 2$). The lengths of the major and minor axes and orientations of individual particles were also quantified using best-fit ellipses. In general, apparent diameters calculated from best-fit ellipses match those determined from the circular cross section defined by their total number of pixels.

The "circular area definition" approach works well for chondrules, which are approximately spherical in shape and likely retain their equidimensionality even when slightly deformed (see Tait et al., 2016). This approach yields more reproducible results for the more irregular shapes of CAIs (*e.g.*, Fig. 2). Particles cut off by the edge of the sample were excluded because their dimensions could not be accurately measured. The data sets were processed using a matrix inversion unfolding algorithm to transform histograms of measured particle diameters into histograms of actual particle diameters (Cuzzi and Olson, 2017, see supplemental Fig. S10). Additionally, for rimmed particles, we measured the apparent diameter of the inner chondrule "**core**" and the apparent diameter including the rim(s) ("**ChonMax**") so that the effective chondrule rim thickness could be seen by comparing **ChonMax** to the "**CoreWRim**" size distributions. Apparent chondrule rim thicknesses were also directly measured on all particles in one of the sample SEM images (see supplemental Table S2) by calculating the average thickness of each rim based on a number of rim measurements determined at different radial orientations.

3. Results

3.1. Particle types

Subpopulations representing the diversity of particles and rims in these meteorites are defined in Table 1. Chondrules are observed to be unrimmed, rimmed, or having two texturally distinct rim layers (an inner coarse-grained rim and an outer fine-grained rim, Fig. 2F). Chondrule data were further subdivided to account for the potential differences between size distributions of rimmed chondrules, or only their cores, to allow comparison of pre- and post-rim formation populations. Each individual particle was digitized as just a core and again including its surrounding rim, if present (see supplemental Fig. S8). Individual particles belong to multiple groupings, *e.g.*, a rimmed chondrule would have a "**Rimmed**" diameter, which reflects the sum of its core and rim, and would be tabulated in the "**ChonMax"** population. This particle would also have a "**CoreWRim**" diameter, *i.e.*, just its "naked" core, which would be included in the "**AllchonCore**" population. An unrimmed chondrule would have a "**CoreNoRim**" diameter and would be included in both the "**ChonMax**" and "**AllchonCore**" populations.

The small "micro-chondrules" (Fruland et al., 1978) that appear to be included within the rims themselves suggest that some of these particles either represent part of the rim formation process and/or were enveloped into a rim forming event. This complicates the counting statistics because there can be more chondrule cores ("**AllchonCore**" $n = 2555$) than individual chondrules "particles" ("**ChonMax**" $n = 2339$) depending on how they are defined. For this reason, we report fewer total particles when we group the instances of multiple small particle cores, embedded within large particle rims, as part of the larger particles (*i.e.*, ChonMax as opposed to AllchonCore). Although these size distributions are similar (Fig. 5A), we consider the ChonMax particle population—which by definition excludes smaller particle cores contained in rims—as the most appropriate to test primary aerodynamic sorting models as

Table 1
Definitions.

Fundamental particle types	
CAI	Ca-, Al-rich refractory inclusion
AOA	Amoeboid Olivine Aggregate, a type of inclusion
PO	Porphyritic Olivine chondrule
POP	Porphyritic Olivine and Pyroxene chondrule
PP	Porphyritic Pyroxene chondrule
BO	Barred Olivine chondrule
RP	Radiating Porphyritic chondrule
CC	Cryptocrystalline chondrule
Chondrule groupings	
ChonMax	chondrule of maximum particle diameter, including rim when present
AllchonCore	individual chondrule core, regardless of rim status—present, absent, or co-shared rim
Rimmed	chondrule particle with rim, including rim
CoreWRim	chondrule particle with rim, excluding rim
CoreNoRim	chondrule particle that lacks rim
Inclusions	CAI and AOA types
Type A CAI	melilite dominated CAI
Type B CAI	pyroxene-melilite dominated CAI
FG rims	fine-grained rims surrounding chondrules, likely accretionary
CG rims	generic coarse-grained rim surrounding chondrules, possibly igneous
WL rims	Wark–Lovering rims surrounding CAIs

The term "core" is used generally to mean the diameter of a particle excluding the additional thickness of its rim, if present. ChonMax, AllchonCore, Rimmed, CoreWRim, and CoreNoRim are different ways to group chondrule subtypes, i.e., individual particles can belong to multiple groups.
Micro-chondrules are not classified as a stand alone group in this work. They are included as appropriate as smaller members of each particle subpopulation, as well as, part of the overall "AllchondCore" size distribution.
When small "micro-chondrules" are embedded within large particle rims, as part of the larger particles they are not counted separately in "ChonMax".

earlier formed rims would contribute to the effective size of the particles during sorting.

Unfolded size distributions are shown for individual particle subpopulations in Fig. 4A–J and shown overlain for comparison in Fig. 5A–D. The characterization of all particles identified, both in SEM X-ray images and in photomosaics of the slabs is summarized in Table 2. Unless stated otherwise, the size distributions denote the number per unit volume of particle cores as a function of the actual unfolded geometric mean diameter without the added thickness of their associated rims. Ultimately, 13 size distribution data sets were selected for which enough data were collected to yield statistically meaningful results and for which we have confidence of accurate particle type grouping. These data sets are: (1) Maximum chondrule diameter (ChonMax, $n = 2339$) that includes the added thickness of rims when present, (2) Chondrule core diameter (AllchonCore, $n = 2555$) regardless of whether they have rims or are in a rim, (3) Inclusion diameter ($n = 195$) all types, (4) Chondrule core diameter of chondrules with no rims (CoreNoRim, $n = 2161$), (5) Chondrule core diameter of chondrules with rims (CoreWRim, $n = 387$), excluding the added thickness of their rims, (6) PO chondrule core diameter ($n = 1306$), (7) POP chondrule core diameter ($n = 1042$), (8) PP chondrule core diameter ($n = 155$), and (9) Type A CAI diameter ($n = 156$) for Allende SEM data, (10) "All particle" diameter for Allende slab ($n = 6530$), (11) Diameter for particles contained only in the light lithology of NWA 5717 slab ($n = 4121$), (12) Diameter for particles contained only in the dark lithology of NWA 5717 slab ($n = 8206$), and (13) "All particle" diameter for NWA 5717 slab ($n = 12{,}966$).

Results for other particle types that are less abundant have been listed in Table 2 for completeness. These include: (1) Type B CAIs ($n = 24$), (2) Amoeboid Olivine Aggregates ($n = 15$), (3) Al-rich chondrules ($n = 21$), and (4) BO chondrules ($n = 31$) from the Allende SEM images. In general, the SEM results are consistent with component particles identified in the photomosaic Allende slab sample, including Types A, B, and AOA inclusions and a variety of petrographically distinct chondrule types.

Ultimately, all of the particle subgroups were combined in the photographed Allende slab analyses because we found that visual distinction between separate particle types became uncertain below ~200 μm, and was inconsistent between the multiple observers. Although CAIs in the Allende slab were generally visible against the dark matrix, the outlines of chondrules proved more difficult to delineate than in the X-ray maps and their frequency appears to have been undercounted due to selection bias at diameters less than ~150 μm. A similar apparent drop in particle counts at the smaller sizes is seen in the NWA 5717 slab data (Fig. 5C).

Modal area percentages from Allende SEM data are derived from the three main components: chondrules (ChonMax, 46.3%), inclusions (3.4%), and matrix (50.3%). The average diameter of each particle subgroup in SEM data is calculated from a nonlinear best fit lognormal curve to each distribution (Fig. 4, see Supplement 13 for details). Average diameters of these particle subgroups vary somewhat, but all populations exhibit broad size ranges. Among chondrules, PO chondrules are the most common (51%, by number), exhibit the smallest average diameter (measured diameter ~150 μm, unfolded diameter ~160 μm), and represent 6% of the total modal area. The POP chondrules are less common (41%, by number), but are on average about 3x larger (measured diameter ~400 μm, unfolded diameter ~490 μm), so make up the largest area fraction of all particles (22%). The PP chondrules are even less common (6%), but large (measured diameter ~380 μm, unfolded diameter ~460 μm) on average, and represent ~4% of the total modal area. Each of the less common chondrule types (BO and Al-rich) appears to represent about 1% of the counts and modal area, and to be relatively large (measured diameter ~700 μm) on average. Overall 2.6% by area are Type A or Type B CAIs and 0.8% are AOA. The Type A CAIs are the most common, but smaller (measured diameter ~200 μm) on average as compared to the Type B and AOA, which on average are about 2–3× larger (measured diameter ~500 to 700 μm). The latter subgroups (Type B CAIs and AOAs along with BO and Al-rich chondrules) have too few sam-

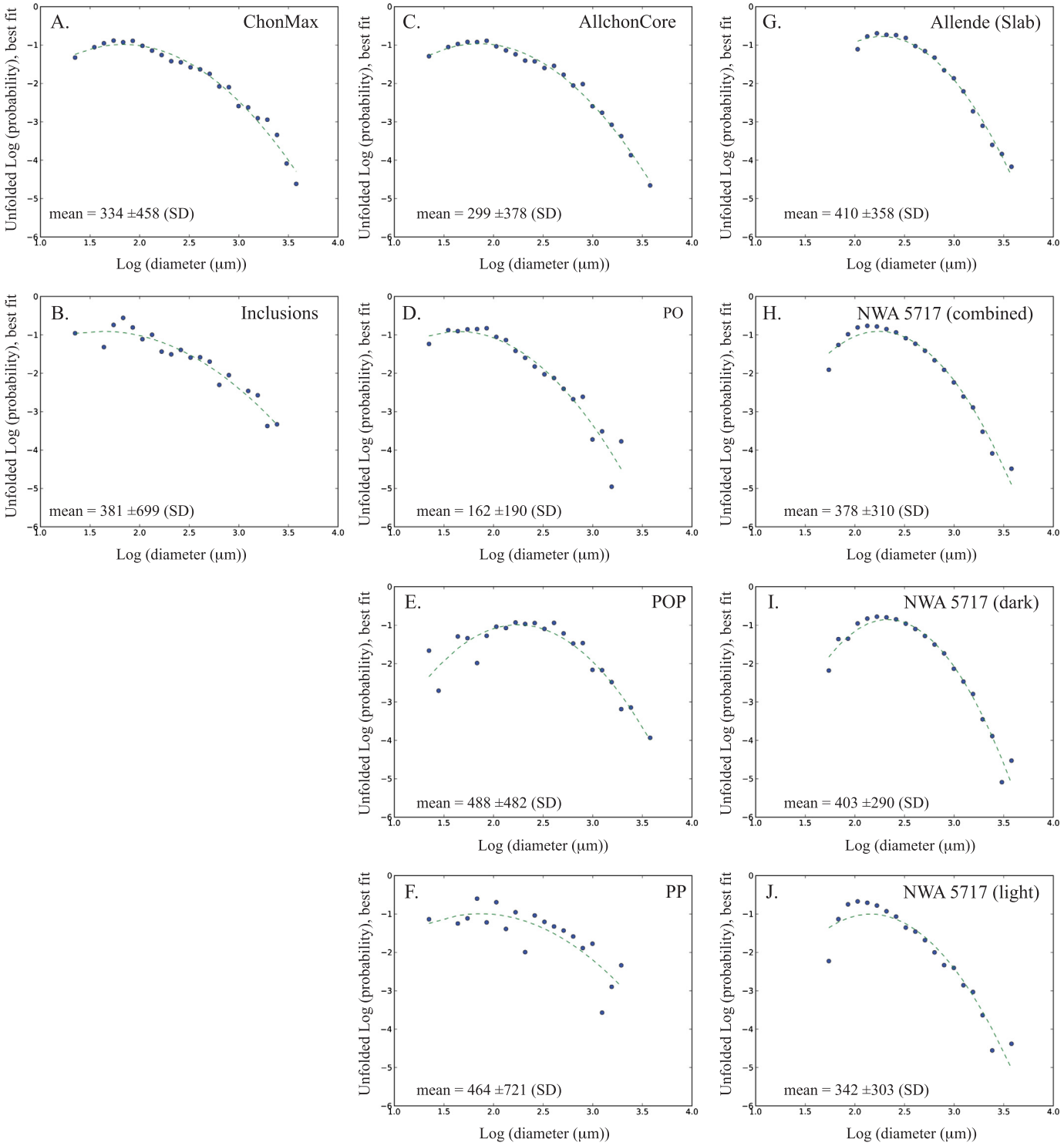

Fig. 4. Nonlinear best fits of lognormal curves to unfolded size particle populations. (A–F) are Allende SEM X-ray images. Subgroup ChonMax is indistinguishable from Inclusions and AllchonCore. AllchonCore is the composite population of PP, PO, and POP that individually define distinct size distribution curves. (G–J) Allende and NWA 5717 slab (photomicrographic) data also exhibit broad distributions, but likely include artifacts of undercounting of the small particle sizes. Particles are binned geometrically where the number per bin is divided by the (variable) bin width to give the number per unit radius. The effect of non-diametric particle sectioning is corrected for in the unfolding calculations (Cuzzi and Olson, 2017).

pled particles to assume that these averages are fully representative.

3.2. Particle rims

No resolvable rims were seen in the NWA 5717 slab. This contrasts with the ∼20% fraction of particles with obvious rims in the Allende slab photomosaic. The thicknesses of rims on Allende chondrules in the SEM data set were evaluated in two ways. Rim widths were estimated indirectly by subtracting ChonWRim sizes from ChonMax sizes, and directly where all individual rim thicknesses were measured in one X-ray image ($n = 413$ particles). In the overall SEM data set and in the single image, where rim thicknesses were directly measured, chondrules with rims represented

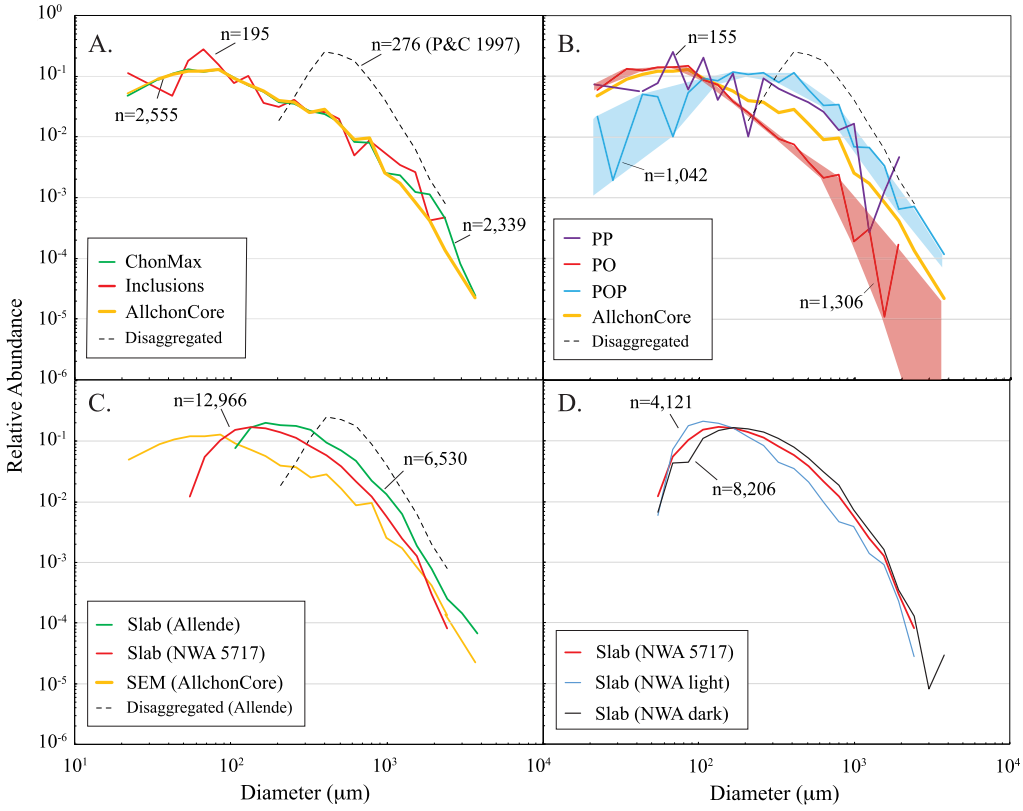

Fig. 5. Unfolded, actual, size distributions of major particle components of Allende and NWA 5717 meteorites. (A) Similar distributions of chondrules and inclusions in Allende are broader than the narrow range of particles disaggregated by Paque and Cuzzi (1997). (B) Distributions of petrographically distinct particle types in Allende (described in Fig. 2). POP chondrule population (blue shaded) contains significantly greater numbers of larger particles than PO chondrule population (red shaded). (C) Photomicrographic slab data of Allende and ordinary chondrite NWA 5717 compared to SEM chondrite cores (AllchonCore) and Paque and Cuzzi data. (D) NWA 5717 light lithology appears to have fewer larger particles than the dark lithology. Particle binning as in Fig. 4. Significant undercounting of smaller particle sizes in slab and disaggregation work exist.

Table 2
Summary of particles characterized in Allende and NWA 5717.

Data set	Particle	Subtype	Avg. diameter (μm)	SD (μm)	Avg. diameter (μm)	SD (μm)	Area (%)	Count
SEM (Allende)	Inclusions		measured		unfolded			
		Type A CAIs	216	270	–		1.4	156
		Type B CAIs	559	583	–		1.2	24
		AOA	673	503	–		0.8	15
		Types A & B	262	347	–		2.6	180
		Inclusions	294	376	380	699	3.4	195
SEM (Allende)	Chondrule							
		PO	149	183	162	190	5.7	1306
		POP	397	339	488	482	22.1	1042
		PP	384	385	464	721	3.6	155
		BO	623	384	–		1.3	31
		Al-rich	598	486	–		1.0	21
		AllchonCore	275	307	299	378	33.7	2555
		ChonMax[a]	310	398	334	458	46.3	2339
SEM (Allende, Image#9)[b]	Chondrule							
		Rimmed	718	662	–			63
		CoreWRim	584	592	–			63
		AllchonCore	366	368	–			350
		ChonMax[a]	379	396	–			413
Slab full section (Allende)	Particles		363	296	410	358	39.1	6530
PaqueAHende set 1 (in Teitler et al., 2010)[c]			*881*	*421*	–			*276*
Slab partial light section (NWA 5717)	Particles[d]		239	238	342	303		4121
Slab partial dark section (NWA 5717)	Particles[d]		328	266	403	290		8206
Slab combined section (NWA 5717)	Particles[d]		295	259	378	310	>95	12,966

ChonMax, AllchonCore, Rimmed, CoreWRim, and CoreNoRim are different ways to group chondrule subtypes, *i.e.*, individual particles can belong to multiple groups.
[a] Indicates particle outer diameter, a sum of "naked" core plus rim that occasionally includes multiple smaller particles.
[b] Particle rim thickness measurements were directly made in SEM Image#9.
[c] Particles derived from sample disaggregation.
[d] Minimal rims present.

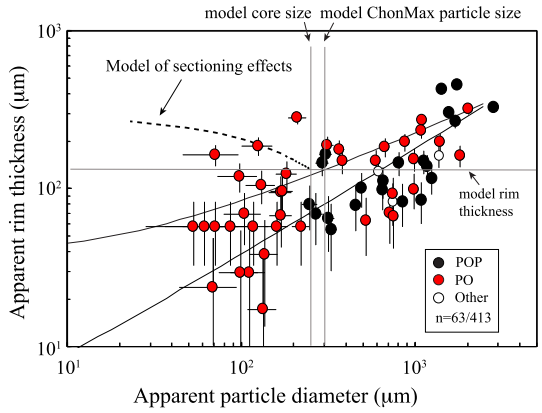

Fig. 6. Log–log plot of chondrule rim thickness versus particle section diameter (CoreWRim) for 1 of 6 X-ray images. Representative models after Cuzzi (2004) that capture the positive trend between core size and rim thickness are shown (solid curves, see Figs. S13 and S14 and Supplement 16). Dashed model curve is the computed apparent rim thickness versus particle diameter from non-diametric slices of an average ~370 μm diameter particle with a uniform 135 μm thick rim. This sectioning model curve is nearly orthogonal to the data trend. Measurement scatter reflects both some 2D sectioning effects shown by the models and precision, which is poorer at the smallest sizes. An estimate for the size measurement uncertainty (±25 μm) is based on multiple, blind measurements of a selection of fine grained features in the SEM images. Unrimmed chondrules ($n = 350$) in image not shown.

a minority of the population (~15%), similar to the Allende slab. Nearly all of the rims are seen surrounding PO and POP subtypes, and of these chondrules, ~1/3 have only fine-grained (FG) rims, ~1/3 have only coarse-grained (CG) rims, and ~1/3 have *both*, with an inner coarse-grained rim overlain by an outer fine-grained rim. No examples of inner fine-grained rims were observed. POP chondrules may have slightly more FG rims (see Table S2). The direct measurements of rim widths on chondrules are shown in Fig. 6, a plot of measured rim thickness versus particle core diameter. Particles without rims are not shown in Fig. 6. Among the measured particles (CoreWRim) there is a positive correlation between particle core diameter and rim thickness, as suggested by Metzler et al. (1992), Morfill et al. (1998), Cuzzi (2004), and Hanna and Ketcham (2018).

3.3. Broad particle size distributions are characteristic of both meteorites

The modal areas determined here for Allende chondrules (~46%) and inclusions (3.4% total, or 2.6% if AOAs are excluded) are generally consistent with the proportions found in previous investigations. Because of the difficulty of distinguishing chondrule subtypes in the slab photomosaics and, through direct evidence for undercounting of smaller (≤200 μm in diameter) chondrules from comparison of the Allende X-ray image data to the Allende slab photomicroscopy data, it is clear that photomicroscopy size distribution data are not fully representative at the smallest sizes. Furthermore, based on the largest particle sizes that have been reported in the literature, we know that neither of our data sets contain the very largest sizes. Despite these complications, in both types of Allende data and in both the dark and light lithologies of NWA 5717, broad, lognormal particle size distributions are found. These observations contrast sharply with most existing studies. This suggests that there are systematic selection bias effects in previous investigations as well, which likely undercount both smaller and potentially larger sized particles to a degree that is significantly greater than in this study.

3.4. Potential bias in existing data sets

Why and how are these data different from existing data sets? The main advantage of the detailed SEM image analysis approach is that no particle larger than ~50 μm goes unaccounted or unidentified. It is not entirely clear why previous data sets derived from 2D images fail to match the new data, but it could be related to sample bias, lower spatial resolution (*i.e.*, use of pre-field-emission scanning microscopy techniques), observer fatigue, and/or inadequate sample area investigated. Existing studies may be biased towards larger sizes because the authors used thin sections that were selected to include larger particles for measurement of elemental or isotopic compositions. Likewise, there are other potential sources of error in the freeze-thaw disaggregation data sets (*e.g.*, Paque and Cuzzi, 1997) where chondrules had to be hand-picked. Disaggregation size data can also be incidental with the initial goal being a composition study in which larger chondrules/CAIs were selected for ease of handling. In addition to excluding the smallest particles and undercounting others (≤500 μm), the mechanical disaggregation process might also destroy smaller particles and possibly particle rims. It has been pointed out that another potential error in the freeze-thaw disaggregation data sets occurs because the 3D particles were only measured in two dimensions (Teitler et al., 2010). Some existing ordinary chondrite data may also be biased towards larger chondrules because larger particles are more likely to have survived metamorphism on the parent body than smaller particles. This should not be a significant issue for the primitive (3.05) ordinary chondrite NWA 5717 in this work.

To further address our concerns that the broad size distributions observed were artificially produced by inclusion of small crystals and/or angular chondrule fragments rather than actual small chondrules, we specifically re-imaged the small-sized particles characterized. Although petrologic identification of ≤50 μm size particles can sometimes be tricky, Fig. 7 shows several high-resolution backscatter electron SEM images representative of small particles (~100 μm) in our data set (*i.e.*, PO chondrules). These clearly show that the small particles are not just fragments, but rather have circular boundaries and reasonable textures and mineralogy (cf. Nelson and Rubin, 2002). Some of the small sections measured will be artifacts of 2D slicing, but our unfolding calculation accounts for this. Furthermore, the proximity of some small sections to other particles (*e.g.*, Fig. 7) preclude them from being artifacts of non-diametric slices of the ≥500 particles typical of other data sets.

Some small particles are found within in the rims of larger particles (shown in Fig. 7D–F). These "micro-chondrule" particles (Fruland et al., 1978) accreted onto other larger chondrules and do not represent small particles that were accreted individually into planetesimals. By emphasizing the **ChonMax** particle sizes, as described earlier, we are effectively excluding the fraction of small particle cores embedding in larger particle rims. The extra steps to revisit the identity of small particles in the data set validates their true independent small-chondrule nature and ultimately justifies the inclusion of these particles in the reported size distributions.

4. Discussion

4.1. Distinct chondrule lithologies in NWA 5717

Dark and light chondrule-rich "lithologies" contained in NWA 5717 (Bigolski et al., 2016; Bunch et al., 2010) have similar looking broad size distributions. Bunch et al. (2010) said they were identical, but our larger data set allows us to address this claim more definitively. In order to measure the similarity, or dissimilarity, of

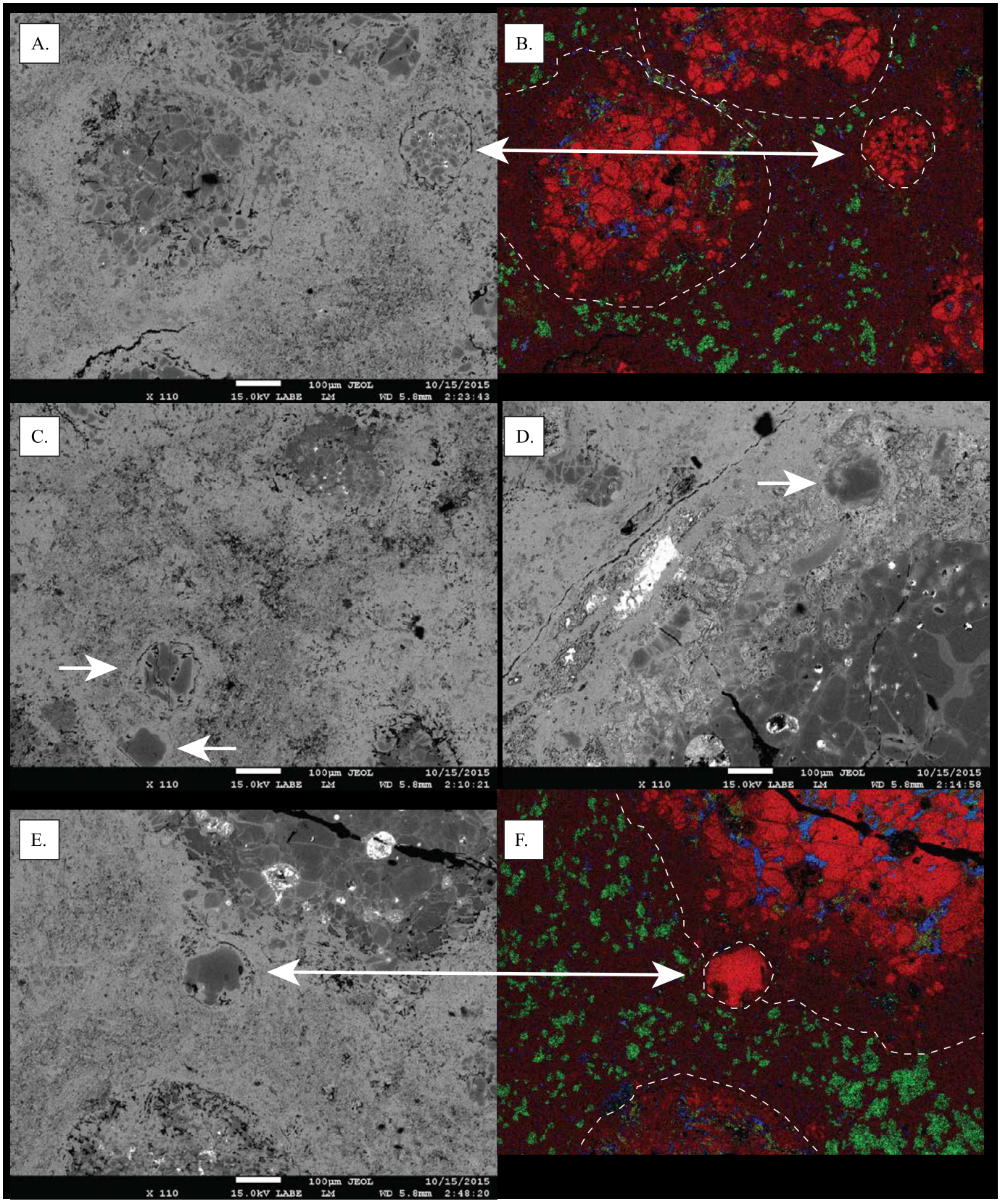

Fig. 7. Representative backscattered electron and X-ray compositional images of small (~100 µm) particles included in this study. RGB color coding as in Fig. 2. Small particles have diverse grain size: (A, B) "micro"-porphyritic and (C–F) porphyritic and/or single crystal chondrules, akin to larger particles. Close proximity of particles shown in A–C attest to the validity of their small size. Particles in D–F appear contained in larger particle accretion rims.

these two distributions we ran several statistical tests (see Supplement 15 for details). Supplemental Table S3 summarizes measures of the probability that the two distributions are the same, based on two different methods, and shown as the $\log_{10}$ of the "odds ratio", which is the probability that the samples are drawn from the same population. An odds ratio near (or larger than) unity would

suggest that two populations are similar. A comparison of the size distribution histograms yields quite negative log odds ratios (see Table S3), therefore, there is strong statistical evidence that they are dissimilar. The first test is an estimation of the Bayesian odds ratio for the two relevant hypotheses, based on a simple root-mean square similarity measure and constant prior (Wolpert, 1995). It is arguably superior to the commonly used Kolmogorov–Smirnov (K-S) test (Press et al., 2007), but we also include K-S probabilities in Table S3. The second test is a straightforward resampling analysis (Efron and Tibshirani, 1993) presented in the form of bootstrap means and standard deviations of the results for both methods. It is clear that both methods overwhelmingly favor the distributions having different shapes (*i.e.*, being drawn from different populations), consistent with their discrepant oxygen isotopes and the incongruity in the magnesium contents of chondrule olivine (Bunch et al., 2010). Put another way, Table S3 says that the probability the dark and light lithology chondrules were drawn from the same population is on the order of 10^{-50} or smaller. This is mostly because their mean sizes are demonstrably different.

Combined with the already known chemical and isotopic differences between the dark and light lithologies (Bunch et al., 2010), these size distribution results strongly suggest that NWA 5717 likely contains an important record of two distinct kinds of chondrule aggregates, each made from chondrules formed with different properties. This in turn indicates that aggregates we see most visibly in the light lithology, but, we hypothesize, also formed the dark lithology, grew by sticking in two separate regions and/or at different times, and then diffused around as aggregates in the nebula until they accreted together into the NWA 5717 parent body and became compacted. In part, the complex internal borders between the dark and light chondrule-rich lithologies likely reflect the aggregate nature of colliding 'clumps' of particles in the nebula. Dark aggregates would have been more numerous so blended together, while the less common light aggregates stand out as "inclusions". The dark lithology appears to be darker in color because of disseminated iron staining. Preliminary Mössbauer spectra (Cato et al., 2017) provide evidence for sulfide and iron metal grains only in the light lithology and not in the dark lithology. One possible explanation of the alteration is *in situ* reaction of metal with nebular ice that originally aggregated only with the (now) dark lithology. This hypothesis is consistent with its relatively "heavy" oxygen isotopic signature (Bunch et al., 2010), along with the diffuse nature of the boundary between the two lithologies. A more thorough examination of the oxygen isotopes within individual chondrules and additional petrologic analysis of the two lithologies could provide important insight into the importance of nebular versus parent body alteration processes.

The statistical analyses (*i.e.*, the large positive log Odds ratios and Boot means in Table S3) also reveal that the *shapes* of the size distributions within the dark and light lithologies, once normalized to a common mean or modal size with a scaling factor (about 1.4–1.5), are the same per the powerful Wolpert analysis (see supplemental Table S4, Fig. S12a). The K–S technique is less certain that this is the case, but there are reasons to favor the Wolpert technique (Feigelson and Babu, 2017). This result could suggest that there is some kind of universality to the processes leading to the aggregation of monomer chondrules into aggregates, in what seem to be two distinct regions with rather different properties. When a similar series of statistical tests are used to compare the shape of the particle size distributions of the NWA 5717 lithologies to that of the Allende slab data (see supplemental Tables S3 and S4) we discover an intriguing result, that *all three* can be "scaled" or normalized to a universal size distribution (shown in Fig. S12b).

4.2. Differences among petrographically distinct chondrule populations

The remainder of our discussion focuses on the data obtained over ~10 cm^2 at the micrometer scale, *i.e.*, the X-ray SEM maps. Similar size distributions of chondrules and refractory inclusions in Allende are depicted in Fig. 5A. The distributions of the most abundant chondrule subgroups detailed in the SEM images are shown in Fig. 5B. The largest differences seen are between POP chondrules ($n = 1042$) that are relatively more abundant at larger sizes and PO chondrules ($n = 1306$) that are relatively more abundant at smaller sizes. The larger mean size of POP chondrules compared to PO likely reflects a difference in their initial formation, perhaps related to additional growth via recondensation (Friend et al., 2016). The third most abundant chondrule subgroup (PP), while noisy (Fig. 5B), defines a distribution that is nearly indistinguishable from the overall broad distributions of inclusions and chondrules (*i.e.*, ChonMax), the latter of which is largely comprised of POP and PO chondrules. It is remarkable, but unlikely to be a coincidence, that when the POP and PO chondrule populations are considered together as one group that they exhibit nearly the same size distribution as PP chondrules and inclusions. Among the inclusion subgroups, Type A CAIs ($n = 156$) are the most common and generally control the distribution. Many of the largest inclusions are Type B CAIs and AOAs, and therefore, both small Type B (±AOA) and large Type A CAIs, are rare and have minimal contributions to the overall distribution. For whatever reason these unobserved particle size fractions did not exist or were preferentially lost prior to particle aggregation and/or parent body accretion.

Abundance differences among petrographically distinct chondrule types have been reported in a number of chondrites. Early work by Gooding and Keil (1981) determined the percentage abundances of chondrule types from L-chondrites and concluded that size and shape are not strictly correlated with chondrule type. Nagahara (1981) obtained a similar result for ALH 77015 (L3.5). Distinct size distributions were reported for different populations in other ordinary chondrites (Gooding, 1983), but the numbers in that study were relatively small ($n = 141$) and the conclusions may not be fully representative. Rubin and Grossman (1987) reported that in EH chondrites ($n = 63$), Radial Pyroxene (RP) chondrules are somewhat larger than Cryptocrystalline (CC) chondrules. They also report that non-porphyritic chondrules have a broader size distribution than porphyritic chondrules and that POP chondrules are significantly larger than PP chondrules. Rubin (1989) found that in CO3 chondrites (11 samples), PO chondrules are on average larger than PP chondrules. More recently, Nelson and Rubin (2002) found that non-porphyritic chondrules are generally larger than porphyritic chondrules ($n = 380$) in Semarkona (CO_3). They concluded that this was due to preferential fragmentation of porphyritic chondrules on the parent body. It is notable that in our work on Allende chondrules, no significant difference was seen in the size distributions as a function of particle circularity ($= 4\pi \times \frac{[area]}{[perimeter]^2}$), which can be used as potential index of fragmentation (see Supplement 14 and Fig. S11). For example, of the ChonMax particles, 2% have circularity <0.35 and these exhibit a measured mean diameter of 358 ± 137 μm (2 SE), as compared to the measured mean diameter of 310 ± 16 μm (2 SE) for all of the ChonMax chondrules.

4.3. Chondrule rims record pre-parent body accretion history

In principle, size sorting could happen after planetesimal accretion (Akridge and Sears, 1999; Bland and Travis, 2017; Nelson and Rubin, 2002), but detailed petrofabric studies of the Allende slab used in this study suggest that these are of secondary importance (Tait et al., 2016). It has also been suggested that rim textures can be produced on the parent body (*e.g.*, Trigo-Rodriguez

et al., 2006). It is not obvious, however, how *in situ* rim formation can produce the positive rim thickness versus particle size relationship observed herein (Fig. 6) or by Metzler et al. (1992), Hanna and Ketcham (2018) or the layering effects observed by Bland et al. (2011), and it certainly has problems explaining the fact that only $\leq$20% of the chondrules in Allende measured in this study have rims.

The fact that a majority of the particles are unrimmed, but hosted in the same meteorite with rimmed particles, supports the notion that individual chondrule subgroups retain signatures of different trajectories on which they evolved separately in space, either by condensation of vapor or by accretion of fine particles on their surfaces, prior to the final accretion event (Morfill et al., 1998). This dichotomy further supports the interpretation that discrete component particles formed and evolved in different nebular environments prior to being caught up in the final sorting regime of planetesimal accretion. A family of model curves was computed following the theoretical approach of Cuzzi (2004) where rim thickness is a function of gas drag stopping time, *i.e.*, larger particles travel further and faster, sweeping up more dust (see Fig. S13 and Supplement 16 for modeling details). Representative "thick-rim" models that capture the positive trend between core size and rim thickness, and some that show the apparent 'leveling off' at small particle diameters (*i.e.*, in PO chondrules), are shown in Fig. 6. Within uncertainty the data and models are consistent with the work of Hanna and Ketcham (2018) on chondrule rims in Murchison, but more data are needed to fully explore potential differences between distinct chondrule subtypes within and among different meteorites.

The evidence indicating thicker chondrule rims on larger particle cores is especially robust after one takes into account the competing effects on the appearance of rim thickness due to sample sectioning artifacts. Rim thicknesses surrounding particles in SEM images tend to be sectioned non-diametrically, like the particles themselves, artificially increasing the rim width at all smaller apparent diameters. If rim thickness is uniform, it should appear thinnest, reflecting its true thickness, on diametric particle cross sections. Therefore, the observed increase in rim thickness as the size of particle cores increases actually underrepresents the increased width of rims surrounding larger particles (*i.e.*, POP chondrules). A simple geometric sectioning model based on the difference between two concentric circles (delta of smaller core and larger rim) that demonstrates the spurious effect on apparent rim thickness in the small non-diametric sections is shown in Fig. 6 (dashed curve). The random sectioning approach of Cuzzi and Olson (2017) was used to generate delta-function size distributions to more comprehensively assess these artifacts (see Fig. S14 and Supplement 16). This modeling indicates that some scatter is unavoidable because of sectioning.

4.4. Theoretical considerations of particle rimming and sorting

Rim formation represents a finite event or events, following condensation or partial melting, during which the particle was coated by dust as it passed through a dusty gas reservoir before it was accreted by sticking into an agglomeration of particles, *e.g.*, Gooding and Keil (1981). The presence of coarse-grained (CG) rims, fine-grained (FG) rims, or both rim types, and varying thickness of rims observed on Allende chondrules, likely reflect time(s) when sufficient dust levels existed in the nebula to rim particles. As chondrules diffused through the nebula they likely encountered a spectrum of heating events, or at least, the ones in the rimming region did so. A common thermodynamic explanation for converting fine-grained minerals to coarse-grained ones by adding heat is Ostwald ripening, in which a dispersed mineral phase is annealed (or texturally matured). Some heating events would be too weak to have a "ripening" effect, and in this scenario the FG rim would be left alone. A stronger event could bake the FG rim to create a CG rim, and the chondrule optionally carries on to accrete a new FG rim. An alternative scenario for CG rim formation is accretion of droplets at the end of the chondrule-forming episode (Jacquet et al., 2013). Whether or not a given particle was ever rimmed, it is clear that strong nebular heating was common enough to melt and/or ablate all or at least the margin of many to generate the ubiquity of "naked" chondrule cores in chondrites.

The presence of turbulence in the protoplanetary disk is one way to explain the thicker rims surrounding larger chondrule cores (Fig. 6). In a turbulent regime, larger particles are predicted to move faster through gas and thus form thicker rims (Cuzzi, 2004). The observed positive correlation (Fig. 6) may also be consistent with numerical studies that suggest their formation in bipolar solar jets where chondrules ejected outwards from the protoSun impacted hypersonically with regions of dusty nebular gas (Liffman and Toscano, 2000). However, it could be explained by any scenario that exposed particles to varying dust/gas and thermal histories (*e.g.*, Connolly and Love, 1998; Morfill et al., 1998), at least for the populations of rimmed chondrules.

The distinct size distributions and rim fractions reported herein (*e.g.*, POP vs. PO), imply that the particles have most likely followed different post-formation histories and their initial size distribution(s) may well have been modified by associated sorting processes in the protoplanetary disk, prior to accretion of the parent body. Sorting processes operating in the early solar nebula have been ascribed to mass (Kuebler and McSween, 1999), differential velocities or turbulent concentration (Cuzzi and Zahnle, 2004), photophoresis (Wurm and Krauss, 2006), X-winds (Shu et al., 1996; Hu, 2010), density (Teitler et al., 2010), or turbulent diffusion (Jacquet et al., 2012), some or all of which may even work simultaneously. All but one of these processes rely on the size-density dependence of aerodynamic drag, and are hypothesized to occur in a number of radial mixing and transport disk models (Cuzzi et al., 2005; Jacquet et al., 2012). The general mechanism of each can be related in principle to observed size distributions (*e.g.*, Teitler et al., 2010), but this relation is not always clear, and may be complicated or overwritten by other processes. If chondrite matrix-chondrule complementarity is valid (Palme et al., 2015), disk-wide sorting may have been more limited. Such a scenario does not preclude the possibility that initially inclusions originated and/or were transported among distinct nebular environments (*e.g.*, Simon et al., 2011) or that chondrules, once formed, and the inclusions where brought together from distinct regions of the protoplanetary disk to make particle aggregates.

4.5. Evidence for nebular particle aggregation

Why the formation of aggregates—which happens by collisions and sticking—seems to manifest some kind of (plausibly aerodynamic) sorting remains unexplained, but supporting evidence can be found in IDPs (Wozniakiewicz et al., 2013), and some hypotheses are being pursued (Cuzzi et al., 2017). The variable internal porosity of aggregates, which may decrease as they approach a bouncing barrier, affects their own aerodynamic stopping times and complicates the situation. The explanations being pursued are not narrow size "filters" but broad ones, consistent with the broad observed particle size distributions (detailed models have not yet been developed). The implication is that the particle size distribution was set during aggregate formation, not planetesimal formation as previously argued by, *e.g.*, Cuzzi et al. (2010).

Our combined findings in Allende and NWA 5717 point to a picture that has the following elements: (1) individual chondrules have an extended lifetime in the nebula as isolated objects, traversing regions with different properties (*i.e.*, dusty regions in which

fine-grained rims can be accumulated, as distinct from regions containing little or no dust; varied thermal environments that act to coarsen or eliminate the pre-existing fine-grained rims). This evolution is probably dominated by turbulent diffusion, and implies some finite radial extent of sampling that depends on nebula turbulent intensity and duration (Cuzzi et al., 2010). (2) On some timescale that is probably longer than the rim accretion timescale (Cuzzi, 2004), based on the Allende mix of rimmed and unrimmed chondrules, chondrules collide and stick with each other, with similar-size particles of other types such as refractory inclusions if present, and maybe clusters of such objects collide with similar-size clusters, to form aggregates that reach fairly large packing fractions, which may reach a "bouncing barrier" limit after which further growth is stalled (Birnstiel et al., 2011; Estrada et al., 2016; Zsom et al., 2010). This stage may be illustrated by at least the light lithology of NWA 5717. However, small porous aggregates such as these still diffuse radially in moderate turbulence without settling, having a diffusion coefficient not much different than their constituent particles (Cuzzi and Hogan, 2003; Youdin and Lithwick, 2007; Jacquet et al., 2012). (3) After some longer time period, associated with radial mixing across wider regions, aggregates of different types may mix and experience the kinds of conditions under which a planetesimal can form. NWA 5717 is unique in that what appear to be constituent aggregates are so qualitatively different as to be readily distinguished. We hypothesize that its dark lithology is composed of similar aggregates in greater abundance, so they simply smear together, suggesting that original (analogous) aggregates forming Allende, for instance, may be currently impossible to distinguish. In Allende, it seems there is no obvious spatial clustering of rimmed versus unrimmed chondrules, so they must have acquired their rims well before ending up in aggregates. We think it is important to test this hypothesis in other primitive chondrites.

If this scenario is correct, the observed chondrule size distributions reflect the size distributions of the components that formed aggregates by sticking, and thus may have been influenced by the probability that a particle can stick, rather than bounce. Regardless of the processes that resulted in the broad—and possibly universal—size distributions, our findings from NWA 5717 (and likely Allende as well) suggest that chondrules can grow by sticking into aggregates of several cm size, and if verified and extended to other objects, this would have profound implications for planetesimal formation.

5. Conclusions

The similar broad size distribution of particle sizes measured across particle subtypes in Allende (*i.e.*, ChonMax and inclusions) suggests that some process size-sorted mineralogically and petrographically diverse refractory inclusions, rimless chondrules, and already-rimmed chondrules collectively prior to their incorporation into the chondrite parent body. These broad size distributions are also seen in the primitive ordinary chondrite NWA 5717, but are different between its two chemically and isotopically distinct lithologies, suggesting the patches of lithology are actually pre-planetesimal aggregates that formed in widely separated regions of the nebula and diffused together prior to planetesimal formation. Some aspect(s) of the aggregate accretion process appears to have over-printed previous, distinct size distributions that existed between particle types (*e.g.*, PO vs. POP); those due to post-formation, pre-planetesimal sorting events. The apparent positive but nonlinear correlation between chondrule size and rim thickness in Allende supports growth of at least some chondrule rims in a turbulent dusty gas reservoir. Collectively, the relatively broad, but noticeably different, lognormal size distributions of the various chondrule subtypes, as well as the presence of distinct rimmed and unrimmed chondrules in Allende, rule out mechanisms that predict single sourced, proximally formed, particle size/type populations, *e.g.*, Johnson et al. (2015). The fact that particle size distributions in both lithologies of NWA 5717 and Allende are very similar in shape after scaling to a common mean size implies the existence of a common, possibly universal, aggregation process. Ultimately, if these size-selective aerodynamic effects allow particle sticking to proceed to larger aggregation sizes than currently expected, the primary formation of planetesimals becomes much easier.

Acknowledgements

The suggestion to explore the thick-rim regime by R. Hanna as well as the helpful review by R. Hanna and a second anonymous reviewer improved this work. Scientific discussions with J.M. Friedrich, D. Ebel, the analytical assistance obtaining X-ray Images by D. K. Ross, and the generous loan of Allende and NWA 5717 meteorite slab samples by P. Mani, J. Minafra, and K. Sliz are greatly appreciated. L. Keller is also thanked for providing one Allende X-ray map. This work is partially supported by NASA grants 11-COS11-66 and 16-EW_2-0163 to J.I.S. and 811073.02.07.03.15, originally from NASA's Origins of Solar Systems Program, to J.N.C. NASA Cosmochemistry (11-COS11-66), Lunar and Planetary Institute internship, and NASA co-op programs supported the summer work of the 6 student authors.

Appendix A. Supplementary material

Supplementary material related to this article can be found online at https://doi.org/10.1016/j.epsl.2018.04.021.

References

Akridge, D.G., Sears, D.W.G., 1999. The gravitational and aerodynamic sorting of meteoritic chondrules and metal: experimental results with implications for chondritic meteorites. J. Geophys. Res. 104, 11853–11864.
Alexander, C.M.O., Grossman, J.N., Ebel, D.S., Ciesla, F.J., 2008. The formation conditions of chondrules and chondrites. Science 320, 1617–1619.
Asphaug, E., Jutzi, M., Movshovitz, N., 2011. Chondrule formation during planetesimal accretion. Earth Planet. Sci. Lett. 308, 369–379.
Bigolski, J.N., Weisberg, M.K., Connolly, H.C.J., Ebel, D.S., 2016. Microchondrules in three unequilibrated ordinary chondrites. Meteorit. Planet. Sci. 51, 235–260.
Birnstiel, T., Ormel, C.W., Dullemond, C.P., 2011. Dust size distributions in coagulation/fragmentation equilibrium: numerical solutions and analytical fits. Astron. Astrophys. 525, A11, 16 pp.
Bland, P.A., Howard, L.E., Prior, D.J., Wheeler, J., Hough, R.M., Dyl, K.A., 2011. Earliest rock fabric formed in the Solar System preserved in a chondrule rim. Nat. Geosci. 4, 244–247.
Bland, P.A., Travis, B.J., 2017. Giant convecting mud balls of the early solar system. Sci. Adv. 3, e1602514.
Boss, A., 1996. Nonaxisymmetry in the solar nebula: disk evolution of giant gaseous protoplanet formation. In: Lunar and Planetary Science Conference, pp. 141–142.
Bunch, T.E., Rumble III, D., Wittke, J.H., Irving, A.J., Pitt, D., 2010. Multilithologic, extra-ordinary chondrite Northwest Africa 5717: further evidence for unrecognized metal-poor, non-carbonaceous chondritic parent bodies. In: Lunar and Planetary Science Conference. Abst. #1280.
Cato, M.J., Simon, J.I., Ross, D.K., Morris, R.V., 2017. Examination of multiple lithologies within the primitive ordinary chondrite NWA 5717. In: 48th Lunar and Planetary Science Conference. Abst. #1964.
Charnoz, S., Aleon, J., Chaumard, N., Baillie, K., Taillifet, E., 2015. Growth of calcium-aluminum-rich inclusions by coagulation and fragmentation in a turbulent protoplanetary disk: observations and simulations. Icarus 252, 440–453.
Ciesla, F.J., 2010. The distributions and ages of refractory objects in the solar nebula. Icarus 208, 445–467.
Connelly, J.N., Bizzarro, M., Krot, A.N., Nordlund, A., Wielandt, D., Ivanova, M.A., 2012. The absolute chronology and thermal processing of solids in the solar protoplanetary disk. Science 338, 651–655.
Connolly, H.C., Love, S.G., 1998. The formation of chondrules: petrologic tests of the shock wave model. Science 280, 62–67.
Cuzzi, J.N., 2004. Blowing in the wind: III. Accretion of dust rims by chondrule-sized particles in a turbulent protoplanetary nebula. Icarus 168, 484–497.
Cuzzi, J.N., Ciesla, F.J., Petaev, M., Krot, A.N., Scott, E.R.D., Weidenschilling, S.J., 2005. Nebular evolution of thermally processed solids: reconciling models and meteorites, chondrites and the protoplanetary disk. In: ASP Conference Series, pp. 732–773.

Cuzzi, J.N., Hartlep, T., Simon, J.I., Cato, M.J., 2017. Aggregates: the fundamental building blocks of planetesimals. In: 48th Lunar and Planetary Science Conference. Abst. #1964.
Cuzzi, J.N., Hogan, R.C., 2003. Blowing in the wind: I. Velocities of chondrule-sized particles in a turbulent protoplanetary nebula. Icarus 164, 127–138.
Cuzzi, J.N., Hogan, R.C., Bottke, W.F., 2010. Towards initial mass functions for asteroids and Kuiper Belt Objects. Icarus 208, 518–538.
Cuzzi, J.N., Hogan, R.C., Paque, J.M., Dobrovolskis, A.R., 2001. Size-selective concentration of chondrules and other small particles in protoplanetary nebula turbulence. Astrophys. J. 546, 496–508.
Cuzzi, J.N., Olson, D.M., 2017. Recovering 3D particle size distributions from 2D sections. Meteorit. Planet. Sci. 52, 532–545.
Cuzzi, J.N., Zahnle, K.J., 2004. Material enhancement in protoplanetary nebulae by particle drift through evaporation fronts. Astrophys. J. 614, 490–496.
Davis, A.M., Zhang, J., Greber, N.D., Hu, J., Tissot, F.L.H., Dauphas, N., 2017. Titanium isotopes and rare earth patterns in CAIs: evidence for thermal processing and gas-dust decoupling in the protoplanetary disk. Geochim. Cosmochim. Acta 221, 275–295.
Desch, S.J., Connolly, H.C.J., 2002. A model of the thermal processing of particles in solar nebula shocks: application to the cooling rates of chondrules. Meteorit. Planet. Sci. 37, 183–207.
Desch, S.J., Cuzzi, J.N., 2000. The generation of lighting in the solar nebula. Icarus 143, 87–105.
Dyl, K.A., Simon, J.I., Young, E.D., 2011. Valence state of titanium in the Wark–Lovering rim of a Leoville CAI as a record of progressive oxidation in the early Solar Nebula. Geochim. Cosmochim. Acta 75, 937–949.
Ebel, D.S., Brunner, C., Konrad, K., Leftwich, K., Erb, I., Lu, M., Rodriquez, H., Crapster-Pregont, E.J., Friedrich, J.M., Weisberg, M.K., 2016. Abundance, major element composition and size of components and matrix in CV, CO and Acfer 094 chondrites. Geochim. Cosmochim. Acta 172, 322–356.
Efron, B., Tibshirani, R., 1993. An Introduction to the Bootstrap. Chapman and Hall, New York.
Estrada, P.R., Cuzzi, J.N., Morgan, D.A., 2016. Global modeling of nebulae with particle growth, drift, and evaporation fronts. I. Methodology and typical results. Astrophys. J. 818. id.200, 241 pp.
Feigelson, E., Babu, J., 2017. Beware the Kolmogorov–Smirnov test! Penn State Astrostatistics and Astroinformatics Portal.
Friedrich, J.M., Weisberg, M.K., Ebel, D.S., Biltz, A.E., Corbett, B.M., Iotzov, I., Kahn, W.S., Wolman, M.D., 2015. Chondrule size and related physical properties: a compilation and evaluation of current data across all meteorite groups. Chem. Erde 75, 419–443.
Friend, P., Hezel, D.C., Mucerschi, D., 2016. The conditions of chondrule formation, part II: open system. Geochim. Cosmochim. Acta 173, 198–209.
Fruland, R.M., King, E.A., McKay, D.S., 1978. Allende dark inclusions. In: Proceedings of Lunar Science Conference 9th, pp. 1305–1329.
Gooding, J.L., 1983. Survey of chondrule average properties in H-, L- and LL-group chondrites—are chondrules the same in all unequilibrated ordinary chondrites? In: Chondrules and Their Origins. Lunar and Planetary Institute, Houston, pp. 61–87.
Gooding, J.L., Keil, K., 1981. Relative abundances of chondrule primary textural types in ordinary chondrites and their bearing on conditions of chondrule formation. Meteorit. Planet. Sci. 16, 17–43.
Grossman, J.N., Rubin, A.E., Nagahara, H., Kring, E.A., 1989. Properties of chondrules. In: Kerridge, J.F., Matthews, M.S. (Eds.), Meteorites and the Early Solar System. Univ. Arizona Press.
Grossman, L., Ebel, D.S., Simon, S.B., 2002. Formation of refractory inclusions by evaporation of condensate precursors. Geochim. Cosmochim. Acta 66, 145–161.
Hanna, R.D., Ketcham, R.A., 2018. Evidence for accretion of fine-grained rims in a turbulent nebula for CM Murchison. Earth Planet. Sci. Lett. 481, 201–211.
Hezel, D.C., Russell, S.S., Ross, A.J., Kearsley, A.T., 2008. Modal abundances of CAIs: implications for bulk chondrite element abundances and fractionations. Meteorit. Planet. Sci. 43, 1879–1894.
Hu, R., 2010. Transport of the first rocks of the solar system by x-winds. Astrophys. J. 725, 1421–1428.
Huang, S., Farkaš, J., Yu, G., Petaev, M., Jacobsen, S.B., 2012. Calcium isotopic ratios and rare earth element abundances in refractory inclusions from the Allende CV3 chondrite. Geochim. Cosmochim. Acta 77, 252–265.
Jacquet, E., Fromang, S., Grounelle, M., 2011. Radial transport of refractory inclusions and their preservation in the dead zone. Astron. Astrophys. 526, L8. 4 pp.
Jacquet, E., Gounelle, M., Fromang, S., 2012. On the aerodynamic redistribution of chondrite components in protoplanetary disks. Icarus 220, 162–173.
Jacquet, E., Paulhiac-Pison, M., Alard, O., Kearsley, A.T., Gounelle, M., 2013. Trace element geochemistry of CR chondrite metal. Meteorit. Planet. Sci. 48, 1981–1999.
Johansen, A., Okuzumi, S., 2018. Harvesting the decay energy of ^{26}Al to drive lighting discharge in protoplanetary discs. Astron. Astrophys. 609, A31. 22 pp.
Johnson, B.C., Minton, D.A., Melosh, H.J., Zuber, M.T., 2015. Impact jetting as the origin of chondrules. Nature 517, 339–341.
Jones, R.H., Lee, T., Connelly, H.C., Love, S.G., Shang, H., 2000. Formation of chondrules and CAIs: theory vs. observation. In: Mannings, V., Boss, A.P., Russell, S.S. (Eds.), Protostars and Planets. University of Arizona Press, Tucson, pp. 927–961.
Joung, M.K.R., Low, M.-M.M., Ebel, D.S., 2004. Chondrule formation and protoplanetary disk heating by current sheets in nonideal magnetohydrodynamic turbulence. Astrophys. J. 606, 532–541.
Kuebler, K.E., McSween, H.Y.J., 1999. Sizes and masses of chondrules and metal-troilite grains in ordinary chondrites: possible implications for nebular sorting. Icarus 141, 96–106.
Levy, E.H., Araki, S., 1989. Magnetic reconnection flares in the protoplanetary nebula and the possible origin of meteorite chondrules. Icarus 81, 74–91.
Liffman, K., Toscano, M., 2000. Chondrule fine-grained mantle formation by hypervelocity impact of chondrules with a dusty gas. Icarus 143, 106–125.
May, E., Russell, S.S., Grady, M.M., 1999. Analysis of chondrule and CAI size and abundance in CO3 and CV3 chondrites: a preliminary study. In: Lunar and Planetary Science Conference. Abst. #1688.
McSween, H.Y., 1977. Petrographic variations among carbonaceous chondrites of the Vigarano type. Geochim. Cosmochim. Acta 41, 1777–1790.
Metzler, K., Bischoff, A., Stöffler, D., 1992. Accretionary dust mantles in CM chondrites: evidence for solar nebula processes. Geochim. Cosmochim. Acta 56, 2873–2897.
Morfill, G.E., Durisen, R.H., Turner, G.W., 1998. An accretion rim constraint on chondrule formation theories. Icarus 134, 180–184.
Morris, M.A., Desch, S.J., 2010. Thermal histories of chondrules in solar nebula shocks. Astrophys. J. 722, 1474–1494.
Morris, M.A., Boley, A.C., Desch, S.J., Athanassiadou, T., 2012. Chondrule formation in bow shocks around eccentric planetary embryos. Astrophys. J. 752, L27. 17 pp.
Nagahara, H., 1981. Petrology of chondrules in ALH-77015 (L3) chondrite. In: Nagata, T. (Ed.), Proceedings of the Sixth Symposium on Antarctic Meteorites. Tokyo, pp. 145–160.
Nelson, V.E., Rubin, A.E., 2002. Size-frequency distribution of chondrules and chondrule fragments in LL3 chondrites; implications for parent-body fragmentation of chondrules. Meteorit. Planet. Sci. 37, 1361–1376.
Palme, H., Hezel, D.C., Ebel, D.S., 2015. The origin of chondrules: constraints from matrix composition and matrix-chondrule complementarity. Earth Planet. Sci. Lett. 411, 11–19.
Paque, J.M., Cuzzi, J.N., 1997. Physical characteristics of chondrules and rims, and aerodynamic sorting in the solar nebula. In: 28th Lunar and Planetary Science Conference. Abst. #071.
Press, W.H., Teukolsky, S.A., Vetterling, W.T., Flannery, B.P., 2007. Section 14.3.3, Numerical Recipes The Art of Scientific Computing, 3rd edition. Cambridge University Press.
Richter, F.M., Davis, A.M., Ebel, D.S., Hashimoto, A., 2002. Elemental and isotopic fractionation of Type B calcium-, aluminum-rich inclusions: experiments, theoretical considerations, and constraints on their thermal evolution. Geochim. Cosmochim. Acta 66, 521–540.
Rubin, A.E., 1989. Size-frequency distributions of chondrules in CO_3 chondrites. Meteoritics 24, 179–189.
Rubin, A.E., Grossman, J.N., 1987. Size-frequency-distributions of EH3 chondrules. Meteoritics 22, 237–251.
Shahar, A., Young, E.D., 2007. Astrophysics of CAI formation as revealed by silicon isotope LA-MC-ICPMS of an igneous CAI. Earth Planet. Sci. Lett. 257, 497–510.
Shu, F.H., Shang, H., Lee, T., 1996. Toward an astrophysical theory of chondrites. Science 271, 1545–1552.
Simon, J.I., Jordan, M.K., Tappa, M.J., Schauble, E.A., Kohl, I.E., Young, E.D., 2017. Calcium and titanium isotope fractionation in refractory inclusions: tracers of condensation and inheritance in the early solar protoplanetary disk. Earth Planet. Sci. Lett. 472, 277–288.
Simon, J.I., Young, E.D., 2011. Resetting, errorchrons and the meaning of canonical CAI initial ^{26}Al/^{27}Al values. Earth Planet. Sci. Lett. 304, 468–482.
Simon, J.I., Hutcheon, I.D., Simon, S.B., Matzel, J.E.P., Ramon, E.C., Weber, P.K., 2011. Oxygen isotope variations at the margin of a CAI records circulation within the solar nebula. Science 331, 1175–1178.
Simon, J.I., Young, E.D., Russell, S.S., Tonui, E.K., Dyl, K.A., Manning, C.E., 2005. A short timescale for changing oxygen fugacity in the solar nebula revealed by high-resolution Al-26–Mg-26 dating of CAI rims. Earth Planet. Sci. Lett. 238, 272–283.
Tait, A.W., Fisher, K.R., Srinivasan, P., Simon, J.I., 2016. Evidence for impact induced pressure gradients on the Allende CV3 parent body: consequences for fluid and volatile transport. Earth Planet. Sci. Lett. 454, 213–224.
Teitler, S.A., Paque, J.M., Cuzzi, J.N., Hogan, R.C., 2010. Statistical tests of chondrule sorting. Meteorit. Planet. Sci. 45, 1124–1135.
Trigo-Rodriguez, J.M., Rubin, A.E., Wasson, J.T., 2006. Non-nebular origin of dark mantles around chondrules and inclusions in CM chondrites. Geochim. Cosmochim. Acta 70, 1271–1290.
Wolpert, D., 1995. Determining Whether Two Data Sets Are from the Same Distribution.
Wood, J.A., 1996. Processing of chondritic and planetary material in spiral density waves in the nebula. Meteorit. Planet. Sci. 31, 641–645.
Wozniakiewicz, P.J., Bradley, J.P., Ishii, H.A., Price, M.C., Brownlee, D.E., 2013. Pre-accretional sorting of grains in the outer solar nebula. Astrophys. J. 779, 164. 166 pp.

Wurm, G., Krauss, O., 2006. Concentration and sort of chondrules and CAIs in the late solar nebula. Icarus 180, 487–495.
Youdin, A.N., Lithwick, Y., 2007. Particle stirring in turbulent gas disks: including orbital oscillations. Icarus 192.
Yu, Y., Hewin, R.H., 1998. Transient heating and chondrule formation: evidence from sodium loss in flash heating simulations experiments. Geochim. Cosmochim. Acta 62, 159–172.
Zsom, A., Ormel, C.W., Guttler, C., Blum, J., Dullemond, C.P., 2010. The outcome of protoplanetary dust growth: pebbles, boulders, or planetesimals? Introducing the bouncing barrier. Astron. Astrophys. 513, id.A57, 22 pp.